Available online at www.sciencedirect.com
SCIENCE DIRECT
ELSEVIER
International Journal of Refrigeration 28 (2005) 605–615
REVUE INTERNATIONALE DU FROID
INTERNATIONAL JOURNAL OF
refrigeration
www.elsevier.com/locate/ijrefrig

Hot gas defrost model development and validation

N. Hoffenbecker, S.A. Klein*, D.T. Reindl

University of Wisconsin—Madison, 1500 Engineering Drive, Madison, WI 53706, USA

Received 20 May 2004; received in revised form 25 July 2004; accepted 30 August 2004
Available online 26 January 2005

Abstract

This paper describes the development, validation, and application of a transient model for predicting the heat and mass transfer effects associated with an industrial air-cooling evaporator during a hot gas defrost cycle. The inputs to the model include the space dry bulb temperature, space humidity, coil geometry, frost thickness, frost density, and hot gas inlet temperature. The model predicts the time required for a complete frost melt as well as the sensible and latent loads transferred back to the conditioned space during the defrost period. The model is validated by comparing predicted results to actual defrost cycle field measurements and to results presented in previously published studies.

A unique contribution of the present model is its ability to estimate parasitic space loads generated during a defrost cycle. The parasitic energy associated with the defrost process includes thermal convection, moisture re-evaporation, and extraction of the stored energy in the coil mass following a defrost cycle. Each of these factors contribute to the parasitic load on compressors connected to the defrost return. The results from the model provide quantitative information on evaporator operation during a defrost cycle which forms the basis to improve the energy efficiency of the defrost process.

Keywords: Air conditioning; Evaporator; Modelling; Heat transfer; Mass transfer; Cycle; Defrosting; Hot gas

Développement et validation d'un modèle pour le dégivrage à gaz chaud

Mots clés : Conditionnement d'air ; Évaporateur ; Modélisation ; Transfert de chaleur ; Transfert de masse ; Cycle ; Dégivrage ; Gaz chaud

1. Introduction

Plate-finned heat exchangers are widely utilized as air-cooling evaporators in industrial refrigeration systems for space conditioning and product cooling. All refrigerant-to-air evaporators operating with coil surface temperatures both below the freezing point of water and dew point temperature of the air within the conditioned space will lead to the formation of frost on the evaporator surface. Frost accumulation on the evaporator has several consequences. First, the accumulation of large amounts of frost will degrade heat transfer performance of the evaporator by fouling the outside surface since, the frost itself has low thermal conductivity (Stoecker [1], Machielsen and Kerschbaumer [2]). With degraded heat transfer performance, evaporator capacity decreases. To meet a specified load with degraded heat transfer performance, the evaporator

* Corresponding author. Tel.: +1 608 263 5626; fax: +1 608 262 8469.

E-mail address: klein@engr.wisc.edu (S.A. Klein).

0140-7007/$35.00 © 2004 Elsevier Ltd and IIR. All rights reserved.
doi:10.1016/j.ijrefrig.2004.08.016

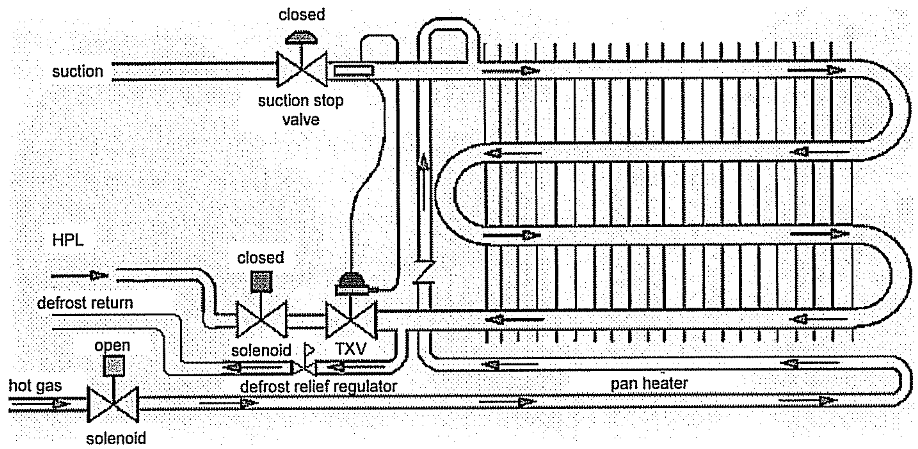

Fig. 1. An evaporator in a hot gas defrost process, Reindl et al. [6].

ammonia, a vapor-only defrost is impractical due to the excessively high gas flow rate requirements since, in this case its extremely high heat of condensation cannot be harnessed for frost melting.

The energy impacts associated with defrosting an evaporator coil depend on the temperature of the refrigerant supplied for the hot gas defrost process and the hot gas dwell time. The lower the refrigerant gas temperature supplied to the coil for defrosting, the lower the rate of sensible and latent parasitic gains to the space but the longer the time period required to achieve a complete melt of the accumulated frost. Higher refrigerant temperatures result in shorter defrost periods but higher rates of sensible and latent gains to the space. Higher refrigerant temperatures also raise the mass of the coil to higher temperatures leading to a greater parasitic cooling load on the refrigeration system following the hot gas defrost process. In either case, longer than necessary defrost dwell times will increase the parasitic load to the space.

Understanding the defrost process is a pre-requisite to making the changes necessary to improve the overall efficiency of the defrost process. The principle contribution of this paper is the development of a mathematical model of the defrost process. The model provides a foundation to understand the energy impacts of the defrost process by quantifying the energy and mass flows involved in the defrost process. The model of the defrost process developed here is compared with available experimental data to validate its performance. The model is then used to investigate the effects of hot gas supply pressure and temperature, hot gas defrost dwell time period, and frost accumulation on evaporators with a goal developing process insights to improve both defrost and refrigeration system efficiency.

2. Modeling the defrost process

Air-cooling evaporators used in industrial refrigeration systems are comprised of a series of multi-row tubes with hundreds of fins pressed over the tubes to enhance heat transfer through the extended surface area. Modeling the defrost process requires consideration of both energy flows and geometry. Due to symmetry, the fin surrounding each tube resembles a hexagon which can be further approximated as a disc, or more appropriately, an annular fin as shown in Fig. 2.

Since, the bulk of frost on an air-cooling evaporator adheres to the finned surfaces, heat needs to be efficiently delivered to the finned surfaces of the coil to melt the frost. During the hot gas defrost process, condensing high pressure refrigerant inside the evaporator tubes warms the tube surfaces which in turn warms the base of each individual fin in contact with the tubes. The fin conducts thermal energy from its base (the tubes) to warm the adhered frost, eventually changing its phase from a solid to a liquid. The bulk of the frost condensate then drains, by gravity, down the coil to the drain pan. Some of the frost evaporates and returns to the conditioned space.

A number of important heat and mass transfer mechanisms arise during the course of a hot gas defrost process: condensation of high-pressure high temperature gaseous refrigerant inside the tubes of the coil; conduction of heat through the coil tubes and fins; sensible heating of accumulated frost; latent melting of accumulated frost; and re-evaporation of moisture from the coil surface to the surrounding space. The following description indicates how the present model incorporates these heat and mass transfer mechanisms.

Fig. 3 illustrates the assumed geometric arrangement for a frosted fin and the associated two-dimensional grid for solving the energy flows during the defrost process. An annular segment of fin forms the basis of the computational domain with a line of symmetry halfway through the fin's thickness. An adiabatic boundary condition is applied at the two lines of symmetry: outer radius of fin/frost and the centerline (right-hand side) of the fin. During the defrost shows the nodal energy balance for a surface node type '*D*'.

$$\underbrace{\rho V\left(\frac{dh}{dt}\right)_{1,j}}_{\dot{E}_{st}} = \underbrace{\left(\frac{k_{1,j-1}+k_{1,j}}{2}\right)2\pi\frac{\Delta x}{2}\frac{(T_{1,j-1}-T_{1,j})}{\ln[(r_i+\Delta r)/r_i]}}_{\text{boundary } a}$$
$$+\underbrace{h_C\pi(r_{j,\text{out}}^2-r_{j,\text{in}}^2)(T_\infty-T_{1,j})+\bar{g}_{m,D}\pi(r_{j,\text{out}}^2-r_{j,\text{in}}^2)(m_{H_2O,s}-m_{H_2O,e})h_{ig}}_{\text{boundary } b}$$
$$+\underbrace{\left(\frac{k_{1,j+1}+k_{1,j}}{2}\right)2\pi\frac{\Delta x}{2}\frac{(T_{1,j+1}-T_{1,j})}{\ln[(r_i+\Delta r)/r_i]}}_{\text{boundary } c}+\underbrace{\left(\frac{k_{2,j}+k_{1,j}}{2}\right)\frac{\pi(r_{j,\text{out}}^2-r_{j,\text{in}}^2)(T_{2,j}-T_{1,j})}{\Delta x}}_{\text{boundary } d} \quad (1)$$

The first term represents the energy stored in the node. Since, each frost control volume experiences a phase change (e.g. from ice to water), the stored energy within the control volume cannot be calculated by using temperature alone. As a result, the energy storage for a frost node is expressed in terms of enthalpy to accommodate the change in phase associated with melting the frost upon sufficient accumulation of thermal energy in the node. The terms identified as 'boundary *a*' and 'boundary *c*' correspond to the thermal conduction from the adjacent nodes at smaller and larger radii, respectively. The term identified as 'boundary *b*' represents the convective heat (first term) and mass transfer (second term) associated with the surrounding environment. The convective heat and mass transfer coefficients are estimated using correlations published by Jaluria [9] and Mills [10], respectively. Lastly, the term identified as 'boundary *d*' represents the thermal conduction between adjacent nodes at the same radial location. Energy balances for other nodes are developed in a similar fashion.

The thermal conductivity of the frost is assumed to be a function of the frost density, as indicated in Eq. (2) from Tao et al. [11] where k_f and ρ_f have units of W/m K and kg/m^3, respectively.

$$k_f = 0.02422 + 7.214\times10^{-4}\rho_f + 1.01797\times10^{-6}\rho_f^2 \quad (2)$$

During the defrost process, the evaporator fans are cycled off and the thermal energy exchange from the evaporator to the surrounding environment is dominated by natural convection. A free convection relationship is used for estimating the Nusselt number and the corresponding natural convection heat transfer coefficient as indicated in Eq. (3) (Jaluria [9]).

$$\overline{Nu}_L = \frac{\bar{h}_C L_{\text{fin}}}{k_{\text{air}}} = 0.13(Ra)^{1/3} \quad \text{for } 10^9 < Ra < 10^{13} \quad (3)$$

In addition to the sensible energy exchange between the coil and the surrounding by natural convection, latent energy transfers occur due to mass transport from vapor pressure differences between the ice (or water) on the coil surface and the surrounding environment. The latent energy transfer rate is proportional to the difference in vapor pressure between the exposed ice (water) surface and the surrounding environment as described by Mills [10]. This driving force for mass transfer can be expressed in terms of mass fractions of water in the air defined as the ratios of the densities of the water vapor in the air at each location divided by the total density of the humid air in each location. The densities are found by using partial pressures related to the saturated pressure at each location. The latent energy transfer rate due to evaporation is given by the following equation.

$$\dot{Q}_{\text{evap}} = \underbrace{\bar{g}_m\pi(r_{\text{out}}^2-r_{\text{in}}^2)(m_{H_2O,s}-m_{H_2O,\infty})h_{ig}}_{\text{boundary } b} \quad (4)$$

The correlation for the mass transfer coefficient, $\bar{g}_m$, expressed in terms of the Sherwood number (Eq. (5)), is given by Jaluria [9] and is shown in Eq. (6) assuming the Lewis Number is unity.

$$\overline{Sh}_L = 0.13(GrSc)^{1/3} \quad \text{for } 10^9 < GrSc < 10^{13} \quad (5)$$

$$\bar{g}_m = \frac{\rho_\infty \nu}{ScL_{\text{fin}}}\overline{Sh}_L \quad (6)$$

The system of discretized equations is then solved in space while using an implicit time integration scheme to establish estimates of the nodal temperatures and heat flows as a function of time during a defrost cycle. One difficulty that arises during a simulated defrost is the effect that the phase change of frost has on the continuity of the computational domain. Rather than attempting to incorporate a methodology to accommodate the solution of a moving boundary domain, the current model approximates the effects of frost melting by assuming that the mass and volume (and thus the density) of each node is constant. When ice melts in the actual evaporator, water drains and the volume formerly occupied by water is replaced by air that has a much smaller mass. The temperature of the air in this nodal space remains relatively constant because of free convection, i.e. air in the freezer space continuously replaces the air in the nodal space. The model assumes

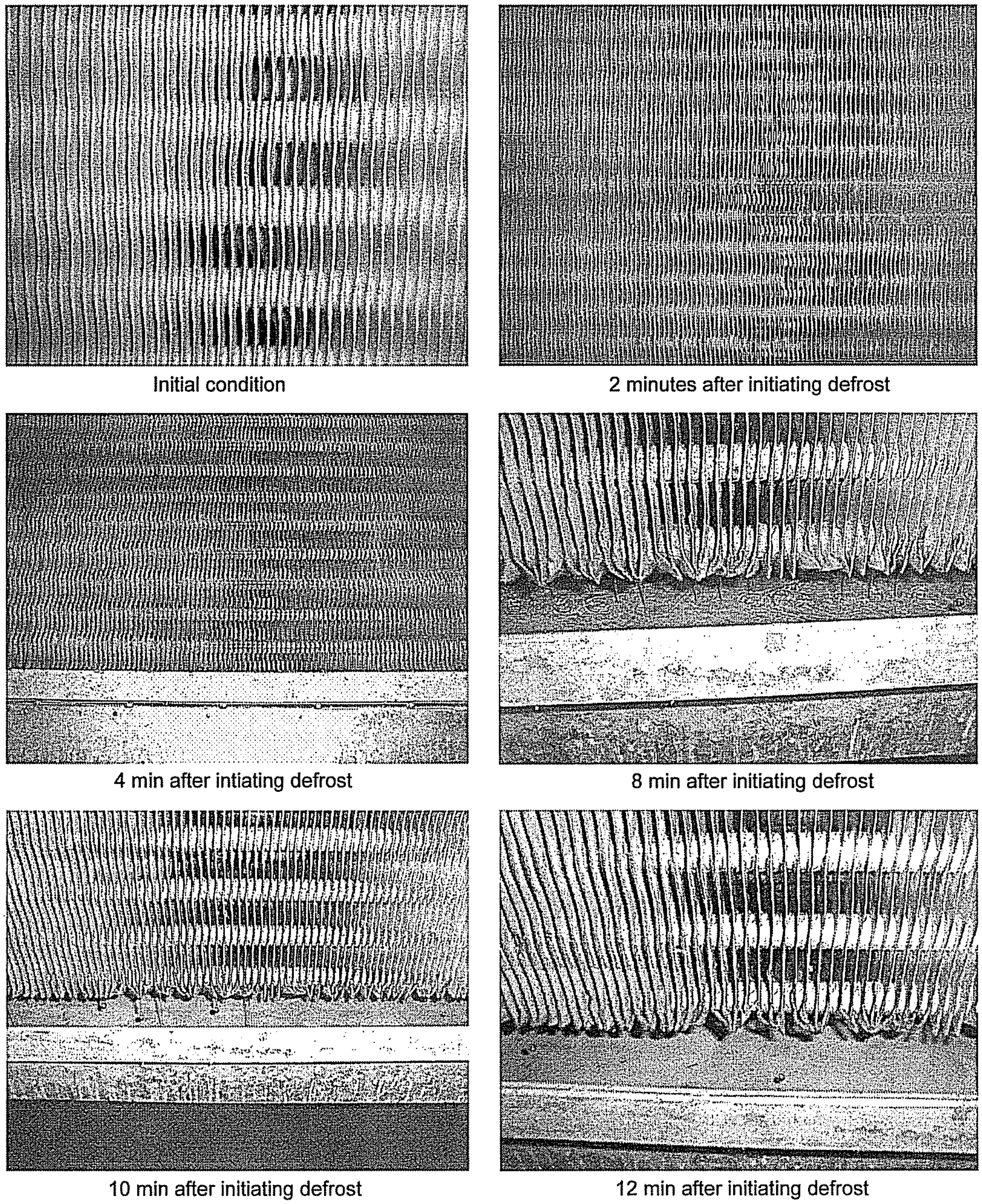

Fig. 4. Visual observation of defrost sequence (Hoffenbecker [12]).

energy input of 28,640 kJ (27,145 Btu). The predicted quantity of energy needed to melt the frost from the coils was 3995 kJ (3786 Btu). Both results compare well with figures reported by Niederer [13].

Stoecker et al. [14] conducted both laboratory measurements of a defrosting evaporator (copper tubes with aluminum fins) using R-22 as well as a field assessment of an evaporator (steel coil with aluminum fins). A thrust of this work was to evaluate whether or not evaporators could be defrosted with low-pressure hot gas with the intent of achieving refrigeration system efficiency improvements. In the laboratory, defrost tests were conducted using a range of hot gas pressures. The evaporator was a six row coil with 14 tubes in each row and fins spaced 0.6 cm (¼ in.) apart across a 71 cm (28 in.) wide span. Table 4 shows an energy budget reported by Stoecker et al. [14] to melt 9.1 kg (20.1 lb_m) of frost from the coil assuming that the condensate is heated to 7 °C (45 F) and the coil is heated to 13 °C (55 F).

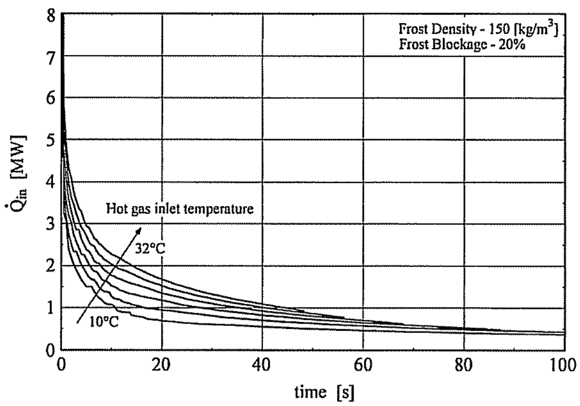

Fig. 5. Rate of supplied energy to the coil during defrost.

Fig. 8 shows the quantity of stored energy in the coil mass (fins and tubes) just after a defrost process terminates. The model assumes that the tubes are entirely heated to the hot gas inlet temperature; however, the fins will have a temperature distribution as determined by the finite difference model. For reference, the defrost times are shown with dotted lines in the figure.

The total quantity of energy supplied during a defrost cycle Q_{in}, represents the integral of the energy supply rate, $\dot{Q}_{in}$, over the entire defrosting period. This energy quantity represents the total amount of energy supplied for defrost, including the losses associated with the stored and released energy. Fig. 9 shows the total energy supplied during defrost along with the time required to fully melt accumulated frost fin are plotted over a range of entering hot gas refrigerant temperatures with frost densities ranging between 150 and 450 kg/m^3 (9.36–28.1 lb$_m$/ft^3) as a parameter and an initial frost blockage of 20%.

As expected, the time to defrost decreases as the hot gas supply temperature increases. However, higher hot gas supply temperatures lead to a higher rate of sensible and latent heat transfer to the surrounding freezer. In addition,

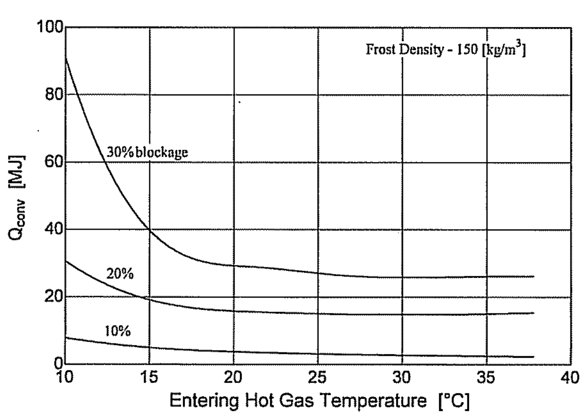

Fig. 6. Total convected energy released during defrost as a function of entering hot gas temperature.

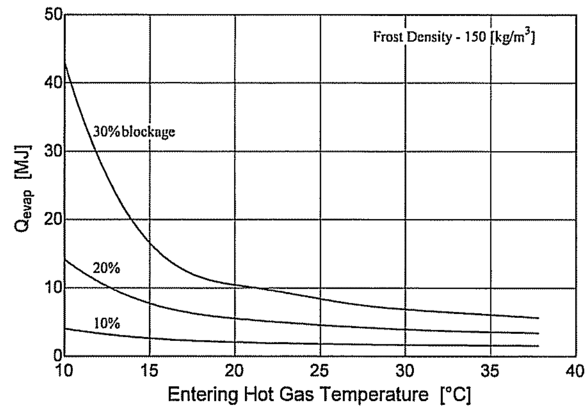

Fig. 7. Integrated latent energy loss during a hot gas defrost cycle as a function of entering hot gas temperature.

the higher hot gas temperatures lead to a greater elevation in coil mass temperature above the melting point of water resulting in a larger energy penalty when the defrost cycle is terminated. The parasitic effects of increasing the hot gas temperature along with the decreasing hot gas dwell time lead to competing factors that result in an optimum (from an energy viewpoint) hot gas inlet temperature. The optimum (minimum) integrated defrost energy input is a function of frost density as shown in Fig. 9. The optimum hot gas temperature for a frost density of 150 kg/m^3 (9.26 lb$_m$ ft^3) is 18 °C (65 F) or just over 689 kPa (100 psig) with ammonia.

Previous studies have focused on achieving defrost with lower hot gas temperatures with the goal of reducing the parasitic load on the space during defrost (Stoecker et al. [14], Cole [15], and Briley [16]). The assumption is that with lower hot gas temperatures, the difference in temperature between the coil and surrounding space will be lower thereby, decreasing the rate of convective heat loss from the coil. In addition, lower hot gas pressures result when systems are run at lower head pressures to improve

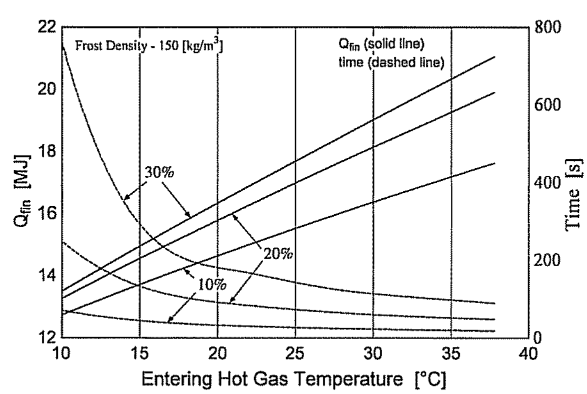

Fig. 8. Stored energy in total evaporator fin surface after the defrost cycle terminates and defrost time as a function of entering hot gas temperature.

Table 7
Defrost efficiency for a set hot gas supply of 45 min for a frost density of 150 [kg/m^3] and frost blockage of 20%

Time	Frost density = 150 [kg/m^3], Frost blockage = 20%					
	37.7 °C 100 F	32.2 °C 90 F	26.7 °C 80 F	21.1 °C 70 F	15.6 °C 60 F	10 °C 50 F
Melt time	48.5 s	56.2 s	1 min 8.2 s	1 min 27.3 s	2 min 5.9 s	4 min 8.6 s
5 min	18.4%	20.2%	22.3%	24.8%	27.7%	30.8%
10 min	12.9%	14.3%	15.9%	18.0%	20.5%	23.4%
15 min	9.9%	11.0%	12.4%	14.1%	16.3%	18.9%
20 min	8.0%	9.0%	10.2%	43.4%	13.5%	15.8%
25 min	6.8%	7.6%	8.6%	9.9%	11.5%	13.6%
30 min	5.8%	6.6%	7.5%	8.6%	10.1%	12.0%
35 min	5.1%	5.8%	6.6%	7.6%	8.9%	10.7%
40 min	4.6%	5.2%	5.9%	6.8%	8.0%	9.6%
45 min	4.1%	4.7%	5.3%	6.2%	7.3%	8.8%

5. Conclusions

A mathematical model for a frosted coil was developed to determine the energy requires for defrosting an evaporator. The frosted coil model is scaled-up based on simulation of the defrost process for a single fin surface. When supplied with the specific geometry and operating conditions, the frosted fin model provided defrost time estimates that compared quite well with the time to melt the accumulated frost that observed at a local cold storage warehouse facility. The model developed also compared well with defrost energy use reported in the literature.

Results from a parametric analysis using the present model showed an optimum hot gas temperature that is a function of both the accumulated mass and density of frost on an evaporator. An interesting result was that the model predicted the mass of moisture re-evaporated back to the space increases with decreasing hot gas temperature. This behavior is due to the prolonged defrost dwell time to achieve a full melt of accumulated frost. The results of this model suggest that parasitic energy impacts associated with the defrost process can be minimized by limiting defrost dwell times.

Acknowledgements

The financial support from the Energy Center Wisconsin is gratefully acknowledged.

References

[1] W.F. Stoecker, How frost formation on coils affects refrigeration systems, Refrig Eng 1957; 42–46.
[2] C.H. Machielsen, H.G. Kerschbaumer, Influence of frost formation and defrosting on the performance of air coolers: standards and dimensionless coefficients for the system designer, Int J Refrig 12 (3) (1989) 283–290.
[3] H. Barrow, A note on frosting of heat pump evaporator surfaces, Heat Recovery Syst 5 (3) (1985) 195–201.
[4] D. Seker, H. Karatas, N. Egrican, Frost formation on fin-and-tube heat exchangers. Part I-modeling of frost formation on fin-and-tube heat exchangers, Int J Refrig 27 (2004) 367–374.
[5] Y. Yao, Y. Jiang, S. Deng, Z. Ma, A study on the performance of the airside heat exchanger under frosting in an air source heat pump water heater/chiller unit, Int J Heat Mass Transfer 47 (2004) 3745–3756.
[6] D.T. Reindl, T.B. Jekel, J.S. Elleson, Industrial refrigeration energy efficiency guidebook, Industrial Refrigeration Consortium, University of Wisconsin—Madison, Madison, WI, 2004.
[7] O.J. Nussbaum, Hot gas defrost without condensing refrigerant, Progress in refrigeration science and technology Proceedings of the XIIth International Congress of Refrigeration, vol. II 1969. p. 1265–1271.
[8] S.A. Klein, F.L. Alvarado, Engineering equation solver. www.fchart.com, F-Chart Software; 2003.
[9] Y. Jaluria, Natural convection, HMT, the science and applications of heat and mass transfer, vol. 5, Pergamon Press, New York, 1980.
[10] A.F. Mills, Heat and mass transfer, Richard D. Irwin Inc, Homewood, IL, 1995.
[11] Y.-X. Tao, R.W. Besant, K.S. Rezkallah, A mathematical model for predicting the densification and growth of frost on a flat plate, Int J Heat Mass Transfer 36 (2) (1993) 353–363.
[12] N. Hoffenbecker. Investigation of alternative defrost strategies. MS Thesis. University of Wisconsin—Madison; 2004.
[13] D.H. Niederer, Frosting and defrosting effects on coil heat transfer, ASHRAE Trans 82 (1) (1976) 467–473.
[14] W.F. Stoecker, J.J. Lux Jr, R.J. Kooy, Energy considerations in hot-gas defrosting of industrial refrigeration coils, ASHRAE Trans 89 (2) (1983) 549–573.
[15] R.A. Cole, Refrigeration loads in a freezer due to hot gas defrost and their associated costs, ASHRAE Trans 95 (2) (1989) 1149–1154.
[16] G.C. Briley. Optimizing defrost systems. Process cooling and equipment; 2003.